Gas Exchange

Evaluation of Local Gas Exchange in a Pulsating Respiratory Support Catheter

Heide J. Eash,* Brian J. Frankowski,* Brack G. Hattler,*† and William J. Federspiel*†‡§

An intravenous respiratory support catheter, the next generation of artificial lungs, is being developed in our laboratory to potentially support acute respiratory failure or patients with chronic obstructive pulmonary disease with acute exacerbations. A rapidly pulsating 25 ml balloon inside a bundle of hollow fiber membranes facilitates supplemental oxygenation and CO_2 removal. In this study, we hypothesized that nonuniform gas exchange in different regions of this fiber bundle was present because of asymmetric balloon collapse and the interaction of longitudinal flow. Four quarter regions and two rings around the central balloon were selectively perfused to evaluate local gas exchange in a 3.18 cm test section using helium as the sweep gas. Quarter region CO_2 exchange rates at 400 beats per minute were 156.8 ± 0.8, 162.5 ± 1.8, 157.2 ± 0.2, and 196.6 ± 0.8 ml/min/m^2 (top, front, bottom, and back, respectively). The back section, adjacent to convex balloon collapse, had 17–20% higher exchange than the other sections caused by higher relative velocities past its stationary fibers. Inner and outer ring maximum pulsation gas exchange rates were 174.4 ± 1.8 and 174.6 ± 0.9 ml/min/m^2, respectively, showing that fluid flow was equally distributed throughout the fiber bundle. *ASAIO Journal* 2005; 51:152–157.

Patients experiencing acute respiratory failure or acute exacerbations of chronic respiratory failure (*e.g.,* chronic obstructive pulmonary disease [COPD]) can potentially be supported through intravenous respiratory assist devices.[1–4] This next generation of artificial lung support, under development but not in clinical use, provides supplemental oxygenation or removal of carbon dioxide through bundles of microporous hollow fiber membranes (HFMs). This technique involves placing the HFM bundle into the vena cava through a peripheral vein (*e.g.,* femoral vein) and connecting the fibers to an external oxygen source.[5] Diffusion gradients are created when pure oxygen flows through the fibers, causing O_2 diffusion into the blood stream and CO_2 diffusion out of the blood (through the gas permeable fiber wall) and into the exhaust gas (mixture of O_2 and CO_2) exiting the device. Placement within the vena cava provides time for the natural lungs to heal because the oxygenation and CO_2 removal is independent of the lungs, which is a benefit over mechanical ventilation,[6,7] the most commonly used therapy. Intravenous respiratory assistance is less complicated than extracorporeal respiratory support because an external blood circuit and pump are not required.

Our group is developing an intravenous respiratory assist catheter to support patients with acute lung failure by improving oxygen delivery and CO_2 removal.[8–12] In its application in patients with COPD, the catheter focuses upon CO_2 removal because oxygenation can be adequately addressed through nasal O_2.[13] Our catheter, seen in **Figure 1**, uses microporous hollow fiber membranes wrapped into a bundle around a pulsating balloon. Pulsation of this centrally located balloon at increasing frequencies creates higher blood velocities past the fiber surfaces than would exist with a passive device. This generates an active mixing environment, in turn facilitating greater gas transfer, subsequently increasing the CO_2 removal capacity of the device.[14] Our previous bench, *ex vivo,* and acute animal testing of our pulsating device[5,10,12] have confirmed that enhanced gas exchange is possible with balloon pulsation[10] when compared with a nonpulsating device, the IVOX.[3,4,15–17]

The balloon within our respiratory assist catheter does not collapse and inflate axisymmetrically. Rather, the balloon collapses asymmetrically into a crescent shape, and the fibers around the balloon move similarly with balloon pulsation in an asymmetric manner. The fibers adjacent to the convex region of the crescent shaped balloon collapse are more stationary during balloon pulsation than the other fiber regions. We hypothesized that asymmetric balloon collapse and inflation within the fiber bundle might cause nonuniform flow patterns and nonuniform gas exchange in different regions of the fiber bundle. We also hypothesized that gas exchange may differ from fibers on the outside of the fiber bundle compared with fibers on the inside of the bundle near the pulsating balloon. To test these hypotheses, we evaluated the local carbon dioxide gas exchange for individual fiber bundle quarters around the central balloon and for inner and outer fiber rings around the balloon (*i.e.,* the inner layer of the fiber bundle closest to the balloon and the outer most layers away from the balloon).

Materials and Methods

This study used a respiratory assist catheter (**Figure 1**) fabricated from 600 microporous hollow fiber membranes (HFMs) (×30–240, Celgard Inc., Charlotte, NC). Ten layers of fibers

From the *Artificial Lung Laboratory, McGowan Institute for Regenerative Medicine, Departments of †Surgery, ‡Chemical Engineering, and §Bioengineering, University of Pittsburgh, Pennsylvania.

Submitted for consideration September 2004; accepted for publication in revised form November 2004.

Correspondence: Dr. William J. Federspiel, University of Pittsburgh, 215 McGowan Institute for Regenerative Medicine, 3025 East Carson St., Pittsburgh, PA 15203.

DOI: 10.1097/01.MAT.0000153648.11692.D0

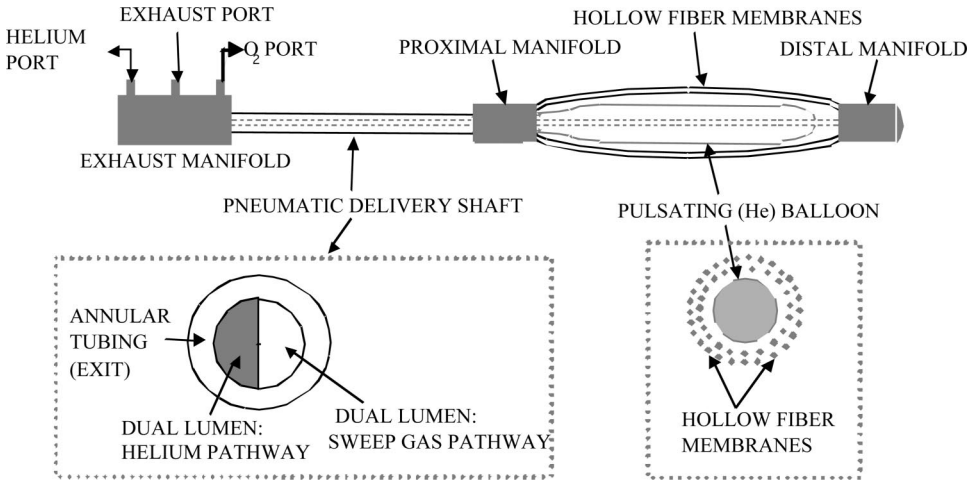

Figure 1. Catheter schematic including cross-sections of pathway tubing and balloon/hollow fiber section.

were wrapped around a 25 ml balloon, when fully inflated creating a 16.5 mm diameter bundle. Fiber surface area was 0.17 m^2 (30 cm in length, 0.030 cm fiber outer diameter, 0.024 cm fiber inner diameter). Dual lumen tubing runs the length of the catheter, which facilitates the sweep gas pathway for gas exchange and helium delivery pathway for the pulsating balloon.

Selective Perfusion Setup

Local gas exchange measurements were performed by selectively perfusing the sweep gas through specific portions of the fiber bundle. Regions were selectively gas perfused by blocking off the sweep gas flow through fibers of nontest regions. **Figure 2** shows a cross-sectional view of the fiber bundle of the device within the test section (outer circle in the figure) in relation to the asymmetric balloon collapse. The fiber bundle is shown as the ring around the collapsed balloon. Solid regions of this fiber bundle are portions that were occluded during selective perfusion testing. The nonsolid areas illustrate open fibers. The catheter used for selective perfusion studies contained a removable distal manifold, which allowed for occluding tape to be placed over the ends of the nontest (nonperfused) fiber regions. The sweep gas (pure oxygen or pure helium) flowed through one side of the dual lumen, then through the fibers, and out through the annular tubing. The pattern allowed for the occluding tape to be pulled into place under vacuum to ensure placement throughout the study (**Figure 1**). This selective perfusion setup was able to determine gas exchange levels in certain sections of the fiber bundle while not causing changes in other aspects of the device. This is a novel approach to looking at artificial lung design; however, a similar technique has been used by Huang *et al.*[18] to study hemodialyzers.

Number of Open Fibers Determination

The number of open fibers in each selectively perfused configuration was determined from the pressure drop *versus* sweep gas flow rate relationship as measured for the perfused region and analyzed as described in a previous publication.[19] Pressure taps were added to the distal and proximal manifolds of the device to measure the upstream and downstream pressures. The device was placed in a column of water at room temperature. Helium was used as the sweep gas to ensure equal gas flow distribution to the fibers in the distal manifold. Sweep gas flow measurements were taken at 0.5 L/min increments (using a thermal mass flow meter, GR-116-A-PV-O2, Fathom Technologies, Round Rock, TX) up to a differential pressure of 250 mm Hg (measured with a pressure transducer, 143SC, SenSym Inc., Milpitas, CA). Upstream and downstream

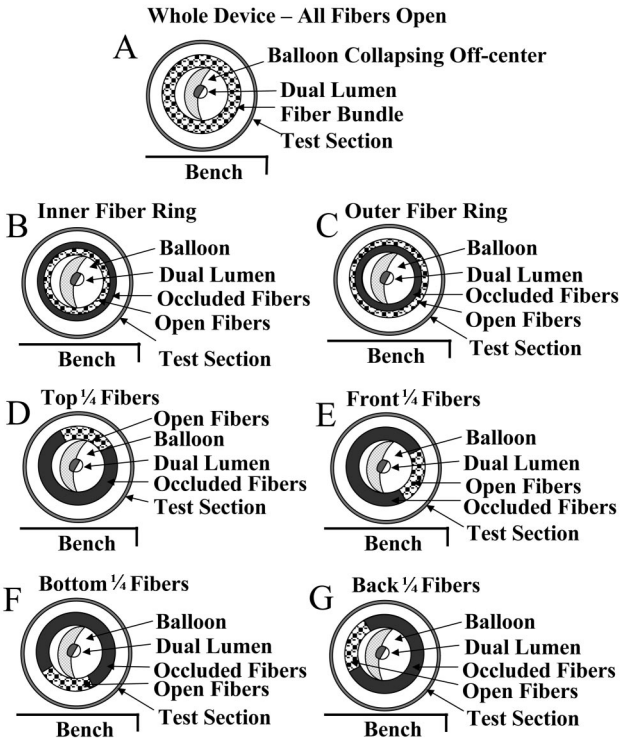

Figure 2. Cross-sectional views of fiber bundle within test section in relation to asymmetric balloon collapse for all selectively perfused configurations.

pressure measurements *versus* flow were used in the compressible Poiseuille flow relationship:

$$P_o^2 - P_I^2 = 2\left(\frac{128\mu L}{N\pi d^4}\right)P_{atm}Q^{RTP} \quad (1)$$

where P_o is the upstream pressure, P_I is the downstream pressure, μ is the fluid viscosity, L is the fiber length, N is the number of open fibers, d is the fiber inner diameter, P_{atm} is the atmospheric pressure, and Q^{RTP} is the sweep gas mass flow rate (in L/min). The difference between the upstream pressure squared and the downstream pressure squared was plotted *versus* sweep gas flow. The slope was used to calculate the number of open fibers for a particular selective perfusion configuration using

$$N = \left(\frac{128\mu L}{\pi d^4}\right)\left(\frac{2P_{atm}}{slope}\right)$$

because μ, L, d, and P_{atm} were constants for a given dataset. This method of determining the number of open fibers in a perfused region was evaluated for accuracy by calculating theoretical $P_0^2 - P_I^2$ values over a range of gas flow rates for the whole device (all fibers open) using **Equation 1**, where N was the physical count of the number of fibers in the device. A physical count was also performed on each selectively perfused region before experimentation to ensure that the calculated number of open fibers was accurate.

Gas Exchange Characterization

All fiber configurations were tested in a mock vena cava loop test setup.[5,9] The sweep gas source was connected to the dual lumen (exhaust) port, pulled through the fiber bundle, and out through the annular (O_2) port (**Figure 1**). The sweep gas was then pulled through a moisture trap, thermal mass flow meter (GR-116-A-PV-O2, Fathom Technologies, Round Rock, TX), and a sealed vacuum pump (400–3910, Barnant Company, Barrington, Illinois). Percentage of CO_2 exiting the device was measured on the positive side of the sealed vacuum pump using a CO_2 analyzer (CO2–44B, Physio-Dyne Instrument Corporation, Quogue, NY). A pressure transducer (143SC, SenSym Inc., Milpitas, CA) was used to measure sweep gas pathway inlet and outlet pressures. The device was placed within a 3.18 cm test section with integral spacers, which kept the device centered in the test section. Deionized water at 37°C was circulated through the loop at 3 L/min. Water flow was set up in a straight configuration without flowing through angled sections before reaching the device. The entire device (*i.e.*, all fibers open) was tested first at a sweep gas flow rate of 3 L/min, and the percentage of CO_2 in the sweep gas exiting the device was recorded at the maximum balloon pulsation rate (400 beats per minute [bpm] for these studies). The sweep gas flow rate of selectively perfused sections was adjusted (from 0.7 to 2.1 L/min, depending upon the test) to achieve this same $\%CO_2$ exhaust found in the whole device while the balloon was at maximum pulsation. This was done to ensure that the diffusion gradient driving forces were the same from one selectively perfused region to another, thus eliminating differences in gas exchange caused by nonuniform driving gradients. Device configurations were tested for gas exchange at various balloon pulsation rates to determine differences, if any, between selectively perfused regions. They were tested first using pure oxygen as the sweep gas, but later repeated using helium as the test gas to explain that any variations in gas exchange performance between sections was not caused by the distribution of sweep gas flow through the distal manifold. The same thermal mass flow meter (GR-116-A-PV-O2, Fathom Technologies, Round Rock, TX) was used for both gases, but with a calibration factor determined before experimentation.

Data Analysis

Gas exchange was quantified primarily in terms of the CO_2 exchange (V_{CO2}) computed from the sweep gas flow rate (Q_{OUT}^{STP}) and CO_2 fraction (F_{CO2}) exiting the selectively perfused regions of the catheter:

$$V_{CO2} = Q_{OUT}^{STP}F_{CO2}$$

The CO_2 exchange (V_{CO2}^*) was normalized to an inlet pCO_2 of 50 mm Hg using:

$$V_{CO2}^* = V_{CO}\frac{50}{pCO_2^{INLET}}$$

to correct for small (< 5 mm Hg) deviations in pCO_2^{INLET} from our target of 50 mm Hg. Gas exchange was also normalized to the fiber surface area for a particular selectively perfused region, using the open fiber number determination described previously.

Statistical Analysis

Statistical comparisons were performed using a Student's t-test, assuming equal sample variance. This method of analysis provided *p*-values for a specific set of comparisons. Differences were considered significant for $0.01 \leq p < 0.05$. P-values of $p < 0.001$ were considered to be very highly significant. Differences were considered not statistically significant for $p > 0.05$, but trending toward statistical significance if $0.05 \leq p < 0.10$.

Results

Carbon dioxide gas exchange (normalized to open fiber surface area) results *versus* balloon pulsation rate for the quarter regions are shown in **Figure 3a** (normalized to an inlet pCO_2 of 50 mm Hg) with pure oxygen. Exchange rates at maximum balloon pulsation (400 bpm) were 166.8 ± 0.2 (top quarter, **Figure 2d**), 169.2 ± 1.2 (front quarter, **Figure 2e**), 160.2 ± 0.2 (bottom quarter, **Figure 2f**), and 188.4 ± 0.4 (back quarter, **Figure 2g**) ml/min/m^2. The top quarter in comparison with the front showed no statistically significant differences (*p*-value = 0.1). The bottom quarter showed a significant statistical difference (*p*-value < 0.008) in comparison with both the top and front regions. There was a significant statistical difference (*p*-value < 0.002) when the back quarter was compared with both the top and bottom quarters, but when compared with the front quarter, $p = 0.002$.

Our hypothesis was that these differences between quarter regions were caused by balloon collapse, but we needed to be sure that gas flow distribution associated with the direction of flow and oxygen as the sweep gas was not the cause. The

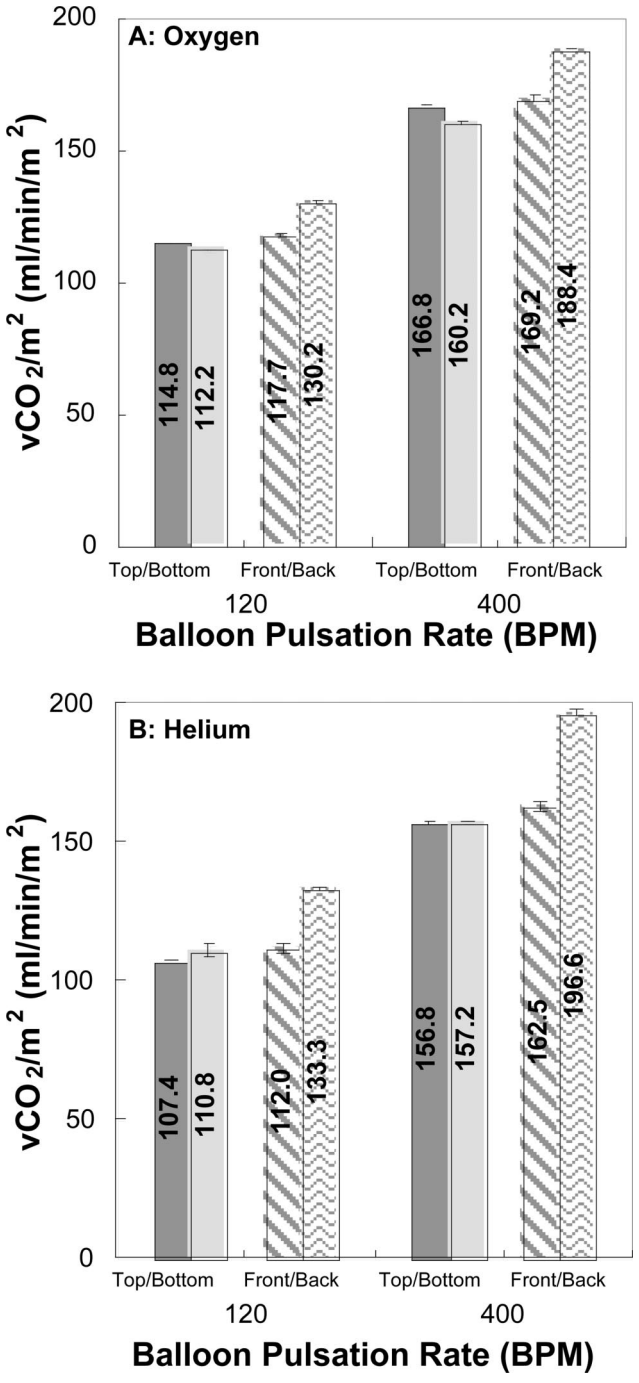

Figure 3. vCO_2 exchange normalized to a pCO_2 of 50 mm Hg for selectively perfused quarter regions *versus* balloon pulsation rate. (A) Oxygen sweep gas; (B) Helium sweep gas.

difference between upstream pressure and downstream pressure squared *versus* sweep gas flow rate is shown in **Figure 4** for the whole device (all fibers open). Experimental measurements are shown in comparison with theoretical calculations (solid lines) for four different sweep gas flow configurations, vacuum source on exhaust, and then oxygen port, using air and then helium as the sweep gas. **Figure 4a** shows experimental *versus* theoretical calculations of the difference between upstream and downstream pressure squared *versus* sweep gas flow rate for the whole device using oxygen. This indicated an 11.5% difference between experimental and theoretical calculations at the maximum sweep gas flow rate tested, leading to the fact that flow distribution cannot be ruled out as a source of the differences in gas exchange between the quarter regions. However, using helium as the sweep gas (**Figure 4b**) showed no difference between theoretical and experimental calculations (*i.e.*, differences in gas exchange between regions were not caused by flow distribution). Thus gas exchange measurements were repeated using helium as the sweep gas to eliminate the possibility that nonuniform flow distribution caused differences in gas exchange.

Three of the four quarters had similar enhancement caused by balloon pulsation when helium was used as the sweep gas (**Figure 3b**). CO_2 exchange rates at the maximum balloon pulsation rate of 400 bpm were 156.8 ± 0.8, 162.5 ± 1.8, and 157.2 ± 0.2 ml/min/m^2 (top, front, and bottom, respectively). However, the back quarter region (**Figure 2g**) had significantly higher gas exchange enhancement because of balloon pulsation when compared with the other quarter regions (p-value $<$ 0.004 for all three other quarter regions *versus* the back quarter). CO_2 exchange at 400 bpm was 196.6 ± 0.8 ml/min/m^2 for this back quarter region. These helium sweep gas exchange rates showed a similar difference between the back region versus other regions as when oxygen was used as the sweep gas (**Figure 3a**).

Figure 5 shows the carbon dioxide gas exchange for the two ring sections, inner (**Figure 2b**) and outer (**Figure 2c**) fibers (normalized to an inlet pCO_2 of 50 mm Hg). The results using oxygen as the sweep gas (with possible nonuniform flow distribution) are shown in **Figure 5a**, and helium sweep gas results are shown in **Figure 5b**. Exchange rates at maximum pulsation were 177.3 ± 0.5 and 177.7 ± 0.5 ml/min/m^2 (O_2 sweep gas) and 174.4 ± 1.8 and 174.6 ± 0.9 ml/min/m^2 (helium sweep gas), inner and outer ring, respectively, yielding no statistical difference between the rings (p-value $>$ 0 .45). Statistically significant differences (p-value = 0.02) were seen at 120 bpm between the inner and outer rings using oxygen as the sweep gas with exchange rates of 123.4 ± 0.3 (inner) and 126.4 ± 0.5 (outer) ml/min/m^2. However, there was no statistically significant difference (p-value = 0.46) between the two rings for this pulsation rate when helium was used as the sweep gas (possibly with flow distribution issues eliminated), with exchange rates of 121.0 ± 1.4 and 121.9 ± 0.5 ml/min/m^2 (inner and outer, respectively). Zero pulsation yielded exchange rates of 12.7 ± 1.4 and 22.7 ± 3.9 ml/min/m^2 (O_2 sweep gas), and 12.2 ± 1.5 and 18.4 ± 1.9 ml/min/m^2 (helium sweep gas) (inner and outer, respectively). This led to a trend toward statistically significant differences between the two rings (p-value = 0.07).

Discussion

This study compared the gas exchange performance of different fiber bundle regions of our current respiratory assist catheter to explore whether nonuniform balloon collapse causes unequal gas exchange in different fiber regions. We looked at the four quarter regions around the balloon (**Figures 2, d–g**), which were oriented with the collapse of the balloon. We concluded that there is a nonuniformity with the "back" quarter region adjacent to the convex region of balloon col-

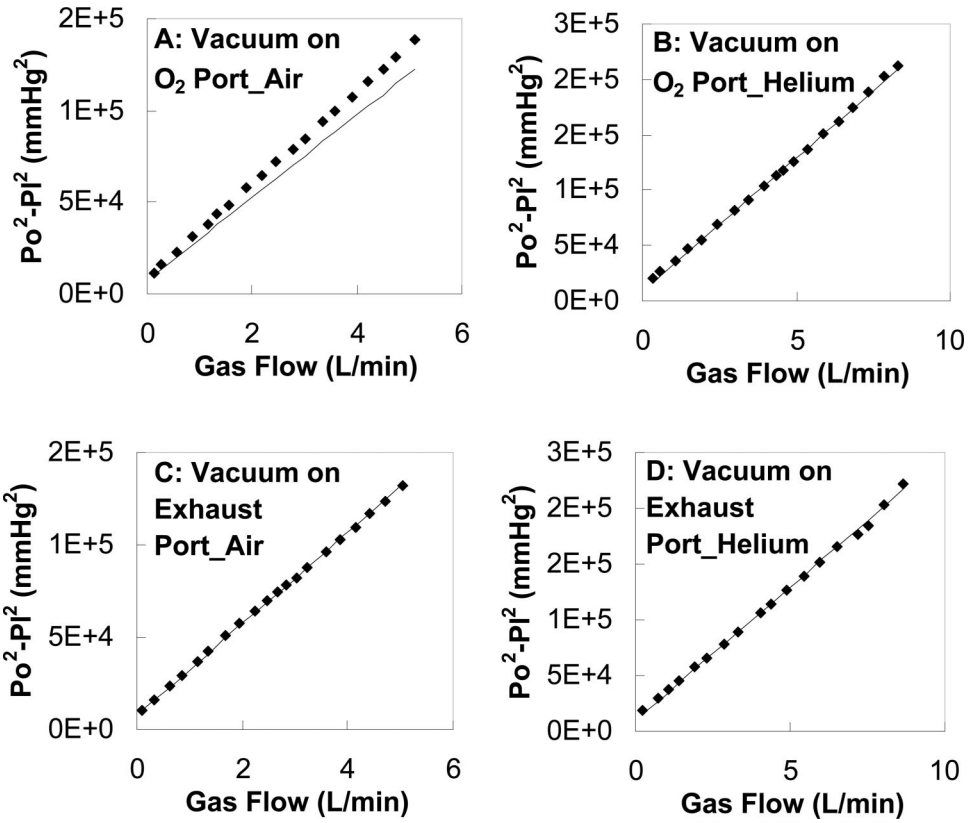

Figure 4. Difference between upstream pressure (Po) and downstream pressure (Pl) squared *versus* sweep gas flow rate for the whole device. Analysis of gas flow distribution for different flow directions and sweep gas. (Solid) Theoretical; (Dotted) Experimental.

lapse (**Figure 3**). We also wanted to examine possible interactions of balloon generated flow with flow past the fiber bundle. We found no differences in gas exchange between the inner and outer rings during balloon pulsation (**Figure 5**).

Eliminating nonuniformities within the test methodology allowed for a true comparison between regions. The difference in gas exchange found between the "back" quarter region and other regions was not caused by liquid flow nonuniformities because the device was centered within the large 3.18 cm test section. Sweep gas flow for this set of studies was pulled first through the dual lumen tubing and then through the fibers. This was done in an effort to ensure that the tape used to occlude the fibers was securely in place throughout the selective perfusion experiments. We evaluated theoretical *versus* experimental measurements for sweep gases with different densities (air and helium) using the number of fibers apparatus discussed previously in methods (**Figure 4**). Experimental values for the less dense helium gas matched up with theory, whereas air did not for this direction of flow (**Figure 4b** *versus* **4a**). Gas exchange comparisons were performed solely upon the CO_2 removal rates (our current focus for clinical use applications of this device) using helium as the sweep gas.

We attributed the difference in gas exchange between the quarter regions to the crescent shaped (*versus* flat) collapse of our balloon. The "back" quarter region (**Figure 2g**) adjacent to the convex side of this collapse showed a 17–20% higher carbon dioxide gas exchange rate as compared with the other three (top, front, and bottom) (**Figures 2d, 2e, and 2f**, respectively). Fibers in the back quarter were more stationary than the other regions as the balloon pulsated. The other fiber regions were in motion with the balloon as it pulsated, that is, having similar velocities. Therefore, the relative fluid velocities past the fibers in these regions were lower than the velocities seen past the back quarter region fibers. The full fluid velocity created by the pulsation of the balloon is seen in this back quarter region. The only difference between the regions was that the fibers on the convex side of the balloon collapse were stationary, and therefore caused the higher gas exchange for the back quarter section.

A key piece of information gathered from these studies is how the balloon collapse influences fiber movement and fluid flow past the fibers. Creating higher relative fluid velocities past the fiber bundle increases the overall gas exchange capability of the device. Our current balloon collapse creates higher velocities in the back quarter region but no other regions. Therefore, our current balloon collapse/fiber bundle combination does not create the high velocities necessary for our targeted higher gas exchange rate of 75–85 ml/min proposed in our most recent NIH grant proposal.[20] We are trying to change the design of our device to increase the velocities of fluid past the hollow fibers. We plan to use flow visualization to analyze fluid flow around the fiber bundle and computational fluid dynamics modeling to make design changes; our institution has experience in using both of these.[21–24] Altering the balloon collapse geometry to interact with the fiber bundle

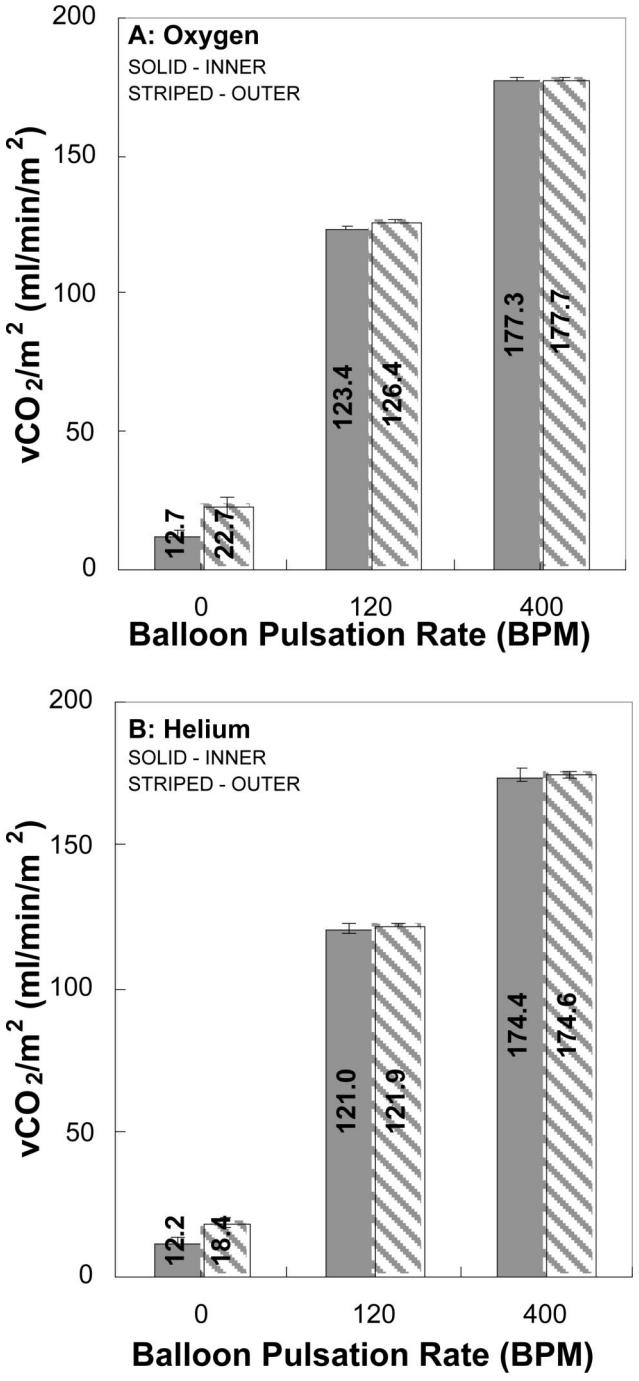

Figure 5. vCO_2 exchange normalized to a pCO_2 of 50 mm Hg for selectively perfused inner and outer rings *versus* balloon pulsation rate. (A) Oxygen sweep gas; (B) Helium sweep gas.

more like the back quarter region in these studies may increase the overall gas exchange.

Acknowledgment

This work was supported by the National Institutes of Health (NIH), National Heart, Lung, and Blood Institute, grant No. HL70051. The views, opinions, and findings contained in this report are those of the authors and should not be construed as an official NIH position, policy, or decision unless so designated by other documentation. The authors thank the University of Pittsburgh's McGowan Institute for Regenerative Medicine for its support.

References

1. Brunet F, Mira JP, Cerf C, *et al*: Permissive hypercapnia and intravascular oxygenator in the treatment of patients with ARDS. *Artif Organs* 18: 826–832, 1994.
2. Conrad SA, Eggerstedt JM, Grier LR, *et al*: Intravenacaval membrane oxygenation and carbon dioxide removal in severe acute respiratory failure. *Chest* 107: 1689–1697, 1995.
3. Durbin Jr. CG: Intravenous oxygenation and CO_2 removal device: IVOX. *Resp Care* 37: 147–153, 1992.
4. Jurmann MJ, Demertzis S, Schaefers HJ, *et al*: Intravascular oxygenation for advanced respiratory failure. *ASAIO J* 38: 120–124, 1992.
5. Hattler BG, Federspiel WJ: Gas exchange in the venous system: Support for the failing lung, in Vaslef SN, Anderson RW (eds), *The Artificial Lung*. Georgetown, TX: Landes Bioscience, 2002, pp. 133–174.
6. Weinacker AB, Vaszar LT: Acute respiratory distress syndrome: Physiology and new management strategies. *Ann Rev Med* 52: 221–237, 2001.
7. Fleury B, Murciano D, Talamo C, *et al*: Work of breathing in patients with chronic obstructive pulmonary disease in acute respiratory failure. *Am Rev Respir Dis* 131: 822–827, 1985.
8. Federspiel WJ, Hout MS, Hewitt TJ, *et al*: Development of a low flow resistance intravenous oxygenator. *ASAIO J* 43: M725–730, 1997.
9. Hattler BG, Federspiel WJ: Progress with the development of the intravenous membrane oxygenator. *Perfusion* 14: 311–315, 1999.
10. Federspiel WJ, Golob JF, Merrill TL, *et al*: Ex vivo testing of the intravenous membrane oxygenator. *ASAIO J* 46: 261–267, 2000.
11. Hattler BG, Lund LW, Golob J, *et al*: A respiratory gas exchange catheter: In vitro and in vivo tests in large animals. *J Thorac Cardiovasc Surg* 124: 520–530, 2002.
12. Eash HJ, Frankowski BJ, Litwak K, *et al*: Acute in vivo testing of a respiratory assist catheter: Implants in calves versus sheep. *ASAIO J* 49: 370–377, 2003.
13. Rosen RL, Bone RC: Treatment of acute exacerbations in chronic obstructive pulmonary disease. *Med Clin North Am* 74: 691–700, 1990.
14. Hewitt TJ, Hattler BG, Federspiel WJ: A mathematical model of gas exchange in an intravenous membrane oxygenator. *Ann Biomed Eng* 26: 166–178, 1998.
15. Mira JP, Brunet F, Belghith M, *et al*: Reduction of ventilator settings allowed by intravenous oxygenator (IVOX) in ARDS patients. *Int Care Med* 21: 11–17, 1995.
16. Mortensen JD: Intravascular oxygenator: A new alternative method for augmenting blood gas transfer in patients with acute respiratory failure. *Artif Organs* 16: 75–82, 1992.
17. Zwischenberger JB, Tao W, Bidani A: Intravascular membrane oxygenator and carbon dioxide removal devices: A review of performance and improvements. *ASAIO J* 45: 41–46, 1999.
18. Huang Z, Klein E, Li B, *et al*: A new method to evaluate the local clearance at different annular rings inside hemodialyzers. *ASAIO J* 49: 692–697, 2003.
19. Federspiel WJ, Williams JL, Hattler BG: Gas flow dynamics in hollow-fiber membranes. *AIChE J* 42: 2094–2099, 1996.
20. Federspiel WJ: *Percutaneous Respiratory Assist Catheter*. National Intitutes of Health, National Heart, Lung, and Blood Institute Grant No. 5R01H070051–03, Apr 1, 2002–Mar 31, 2006.
21. Kerrigan JP, Yamazaki K, Meyer RK, *et al*: High-resolution fluorescent particle-tracking flow visualization within an intraventricular axial flow left ventricular assist device. *Artif Organs* 20: 534–540, 1996.
22. Wu ZJ, Antaki JF, Burgreen GW, *et al*: Fluid dynamic characterization of operating conditions for continuous flow blood pumps. *ASAIO J* 45: 442–449, 1999.
23. Gage KL, Gartner MJ, Burgreen GW, *et al*: Predicting membrane oxygenator pressure drop using computational fluid dynamics. *Artif Organs* 26: 600–607, 2002.
24. Gartner MJ, Wilhelm CR, Gage KL, *et al*: Modeling flow effects on thrombotic deposition in a membrane oxygenator. *Artif Organs* 24: 29–36, 2000.